ACS APPLIED MATERIALS & INTERFACES

Research Article

Cite This: ACS Appl. Mater. Interfaces XXXX, XXX, XXX−XXX

www.acsami.org

Ultrasensitive Microfluidic Paper-Based Electrochemical Biosensor Based on Molecularly Imprinted Film and Boronate Affinity Sandwich Assay for Glycoprotein Detection

Xiaolu Sun,[†,‡] Yannan Jian,[†,‡] He Wang,[†,‡] Shenguang Ge,[*,†] Mei Yan,[*,‡] and Jinghua Yu[‡]

[†]Shandong Collaborative Innovation Center of Technology and Equipements for Biological Diagnosis and Therapy, Institute for Advanced Interdisciplinary Research, University of Jinan, Jinan 250022, P.R. China

[‡]School of Chemistry and Chemical Engineering, University of Jinan, Jinan 250022, P.R. China

Supporting Information

ABSTRACT: In this work, we proposed a strategy that combined molecularly imprinted polymers (MIPs) and hybridization chain reaction into microfluidic paper-based analytical devices for ultrasensitive detection of target glycoprotein ovalbumin (OVA). During the fabrication, Au nanorods with a large surface area and superior conductibility were grown on paper cellulosic fiber as a matrix to introduce a boronate affinity sandwich assay. The composite of MIPs including 4-mercaptophenylboronic acid (MPBA) was able to capture target glycoprotein OVA. SiO_2@Au nanocomposites labeled MPBA and cerium dioxide (CeO_2)-modified nicked DNA double-strand polymers (SiO_2@Au/dsDNA/CeO_2) as a signal tag were captured into the surface of the electrode in the presence of OVA. An electrochemical signal was generated by using nanoceria as redox-active catalytic amplifiers in the presence of 1-naphthol in electrochemical assays. As a result, the electrochemical assay was fabricated and could be applied in the detection of OVA in the wide linear range of 1 pg/mL to 1000 ng/mL with a relatively low detection limit of 0.87 pg/mL (S/N = 3). The results indicated that the proposed platform possessed potential applications in clinical diagnosis and other related fields.

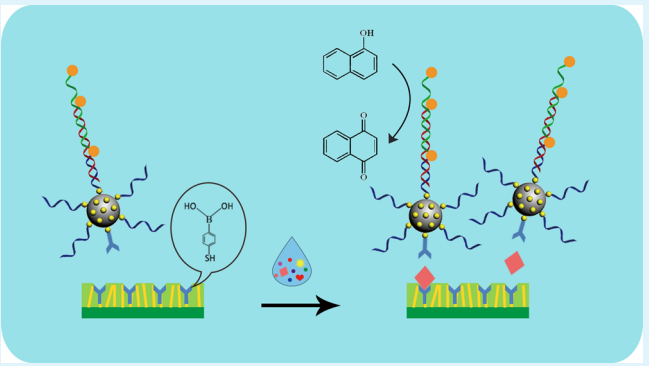

KEYWORDS: *glycoprotein, molecularly imprinted film, boronate affinity sandwich assay, hybridization chain reaction, electrochemical sensor*

1. INTRODUCTION

An oligosaccharide chain which covalently attached to polypeptide side chains exists in the glycoproteins.[1,2] Glycoproteins play a crucial role in various biological events, such as the growth control, division and signaling of cells, and cell migration.[3−6] Protein glycosylation is the most vital post-translational modification for humans, and the occurrence of diseases is strongly associated with the glycoprotein level.[7,8] Therefore, a variety of glycoproteins have been identified as biomarkers in clinical diagnosis.[9] The recognition and detection of glycoproteins requires accurate recognition, high selectivity, and excellent sensitivity because of high levels of interfering substances and low glycoprotein concentrations in complex biological samples.[10] Therefore, improving the selectivity and sensitivity of glycoprotein assay is a significant requirement for clinical diagnosis and treatment. Molecular imprinting is a powerful technique to mimic molecular recognition by natural receptors, which possess antibody-like binding properties or enzyme-like catalytic activities.[11,12] Because of good recognition capacity, easy synthesis, and high chemical stability, molecularly imprinted polymers (MIPs) have been used for chromatographic separation,[13] molecular sensing,[14] drug delivery,[15] and bacteria killing.[16] However, imprinting of biomacromolecules is challenging under harsh imprinting conditions because of the complex imprinting protein structure and large size of the protein. In order to overcome these problems, various approaches have been proposed to achieve in protein imprinting including surface imprinting,[17] hierarchical imprinting,[18] metal-chelating imprinting,[19] and epitope imprinting.[17] Boronate affinity-based MIPs as a promising method have been widely applied in surface imprinting,[20−22] which exhibited excellent specificity, high affinity, widely binding pH range, and excellent anti-interference. Because of these highly beneficial merits, boronate affinity-based MIPs prepared by this approach can be adopted for substituting real antibodies in complex real samples.[9]

Received: January 30, 2019
Accepted: March 20, 2019
Published: March 20, 2019

DOI: 10.1021/acsami.9b02005
ACS Appl. Mater. Interfaces XXXX, XXX, XXX−XXX

Scheme 1. Schematic Illustration of the Proposed Approach for the Detection of Glycoprotein: (A) Preparation of the SiO_2@Au/dsDNA/CeO_2 Signal Tag; (B) Synthesis of the Boronate Affinity-Based Glycoprotein Imprinted Film; and (C) Fabrication Procedure of the Sensing Platform and the Electrochemical Detection of OVA

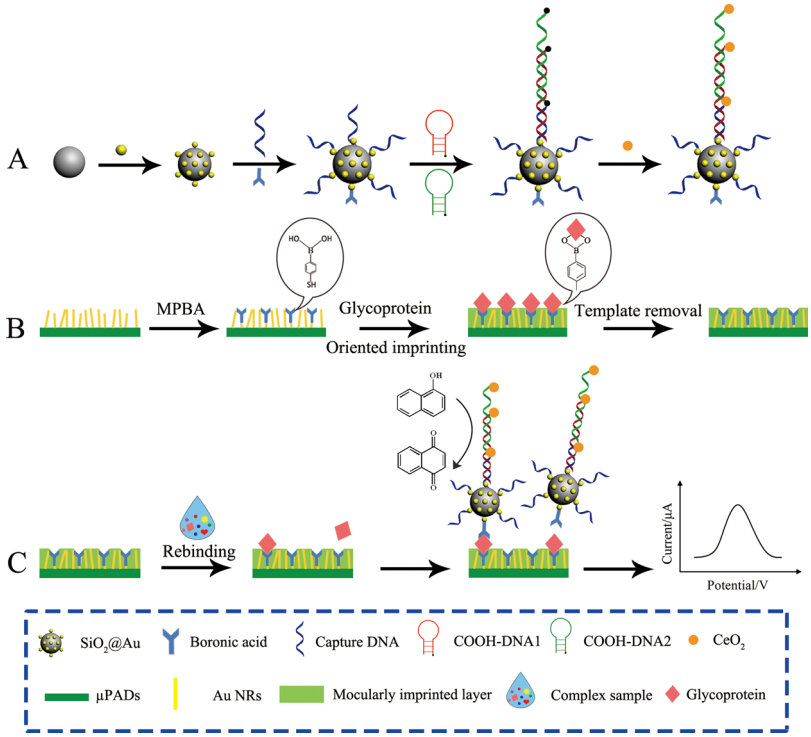

Paper has been widely applied in printing, writing, and wrapping because of its low cost, mass producibility, and disposability. In addition, paper is an attractive platform for bioanalytical applications.[23−25] The first patterned two-dimensional and three-dimensional microfluidic paper-based analytical devices (μPADs) were proposed by the Whitesides group.[26,27] The μPADs have shown a promising prospect for constructing a sensing platform.[28] The spontaneous liquid flow on μPADs is driven by capillary action in the presence of the cellulose matrix, and it avoids the use of any pumping equipment or external power supply. Considering the above benefits toward the μPADs, we synthesize boronate affinity-based MIPs on the μPADs for glycoprotein analysis.

At present, various strategies have been introduced into sensors for achieving high sensitivity. Hybridization chain reaction (HCR) is one of the most attractive enzyme-free amplification processes where an initiator can trigger a hybridization event between the two species of DNA hairpin probes to polymerize into a long nicked double-stranded (dsDNA) structure.[29−31] Therefore, HCR has shown to be an ideal choice in signal amplification because of the benefits of not requiring any enzymes. In addition, signal amplification can be achieved by the nanomaterial, which can catalyze related substrates to accelerate electron transfer in order to enhance sensitivity of this approach.[32,33] Ceria known as the "oxygen reservoir" has attracted extensive research interest in bio-sensing because of its unique properties such as adsorption properties, lattice expansion, shifts in Raman allowed modes, and formation of oxygen vacancies.[34−36] Recently, ceria-based electrochemical sensors have been developed to detect different kinds of substances, including alkaline phosphatase (ALP)-generated products.[37] 1-Naphthol as one of the commonly used ALP-generated products can be oxidized in the presence of nanoceria. The Ce^{4+} ions present in the nanocrystalline ceria can be converted to Ce^{3+}.[34,38] In order to further achieve the signal amplification, Au NPs were doped on the SiO_2 nanoparticle (SiO_2 NPs) surface to form SiO_2@Au nanocomposites. SiO_2@Au could furnish plenty of Au NPs to anchor more dsDNA, which significantly enhanced the electrochemical signal.

Herein, we prepared boronate affinity-based MIPs and SiO_2@Au/dsDNA/CeO_2 composite to fabricate an ultrasensitive sensing platform for rapidly and accurately detecting glycoproteins. There were two favorable methods introduced into this strategy for signal amplification to fabricate an electrochemical sensor, including the preparation of SiO_2@Au and introduction of HCR. It was worth mentioning that the excellent selectivity was obtained because of the introduction of MIPs. Scheme 1 illustrates the construction process of the proposed sensor. First of all, the signal tag SiO_2@Au/dsDNA/CeO_2 was prepared. Au NPs were immobilized to the surface of SiO_2 by the in situ method and subsequent functionalization of nanoparticles by 4-mercaptophenylboronic acid (MPBA) and capture DNA. The preparation of SiO_2@Au not only achieved higher electron transfer efficiency, but also provided a large surface area to anchor more DNA capture for subsequent HCR to further allow signal amplification. Subsequently, the dsDNA formed on the surface of SiO_2@Au through HCR in the presence of two hairpin DNAs. Numerous CeO_2 nanoparticles as electrochemical indicators could be efficiently binding with dsDNA through an amidation reaction. The synthesis of boronate affinity-based MIPs is shown in Scheme 1B. Au nanorod (NR) layer was immobilized on the μPAD surface based on the in situ growth mechanism, and then MPBA was introduced to the electrode surface through the Au−S bond for capturing target glycoprotein. After the

DOI: 10.1021/acsami.9b02005
ACS Appl. Mater. Interfaces XXXX, XXX, XXX−XXX

formation of the imprinting film to achieve the successful preparation of MIPs, the template was removed. Interestingly, the generation of double recognition was beneficial to improve the selectivity of detecting glycoprotein. On the one hand, MIPs could effectively recognize target glycoprotein in the presence of a covalent cyclic ester between boronic acids and glycoprotein. In addition, 3D molecular imprinted cavities matching the shape of target enhanced the selectivity of proposed assay. Therefore, excellent affinity for the target glycoprotein endowed the sensing platform with excellent selectivity. The fabrication of the MIP-based immunosandwich assay is exhibited in Scheme 1C. MIPs could accurately recognize target glycoprotein from complex samples owing to its excellent selectivity. The signal tag was labeled on the electrode surface because of the specific recognition between MPBA present in the signal tag and the target glycoprotein. The Ce^{4+} ions could be converted to Ce^{3+} in the 1-naphthol solution, and the addition of redox-active nanoparticles facilitates conversion of 1-naphthol to naphthoquinone. Thereby, a catalytically amplified signal could be observed in the presence of target glycoprotein ovalbumin (OVA).

2. EXPERIMENTAL SECTION

2.1. Design and Fabrication of μPADs. The μPADs were fabricated by previously reported work with slight modification for glycoprotein detection (Figure S1, details in the Supporting Information).[39] As shown in Scheme 2, this μPADs which fabricated through wax-printing composed of channel tab, detection tab, and washing tab. The hydrophilic circle with the diameter of 8 mm on the detection tab was the sampling zone, on which the counter electrode and working electrode as well as reference electrode were screened-printed. The sample zone was a specific zone where the reaction occurred on the paper. The rest circle with 5 mm diameter was the inlet zone. The assay begins by injecting the solution into the inlet zone for detecting glycoprotein. On the channel tab, the circles were perforated for constructing the channel. The light yellow rectangle area connected the sample zone and washing tab during the washing process, and its semi-hydrophilic property prevented the detection area from being contaminated by the washing liquid. Furthermore, the washing tab was the hydrophilic zone to absorb excess solution. After folding along with line 1, the semi-hydrophilic zone connected the sample zone and washing tab. When washing buffer was added to the sample zone, semi-hydrophilic zone brought excess solution into the washing tab. Furthermore, the hydrophobic side protected the detection tab from the washing liquid contamination. After folding along with line 2, the channel was slipped down onto the three electrodes such that it brought the three electrodes into electrochemical contact. A small drop of buffer was added to the inlet, which wet the sample zone, and a differential pulse voltammetry (DPV) or cyclic voltammograms (CV) measurement could be obtained.

Scheme 2. Obverse (A) and the Reverse (B) of Schematic Representation, Size, and Shape of μPADs; the Obverse (C) and the Reverse (D) of the Fabrication of μPADs for Detection of OVA; the Operation Process of μPADs for (E) Washing and (F) Detecting

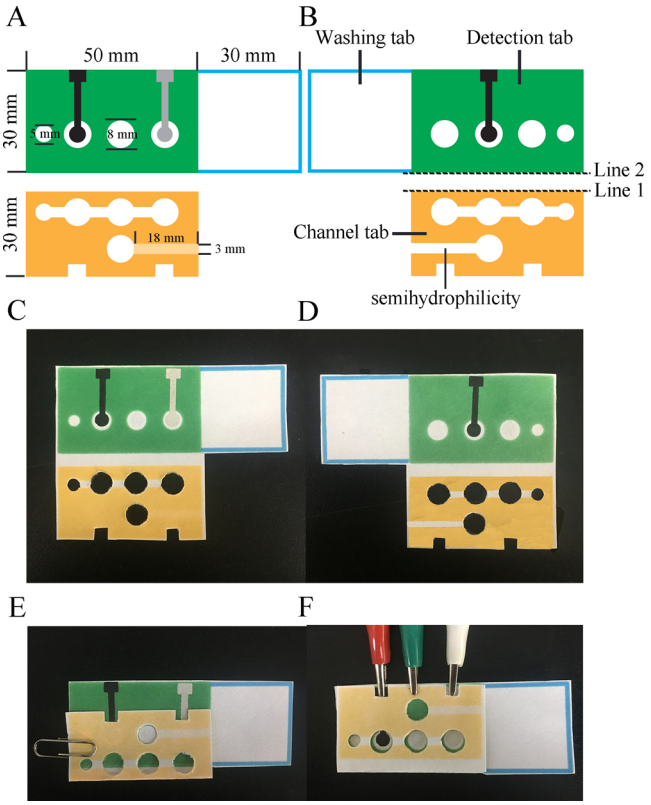

2.2. Preparation of the SiO_2@Au/dsDNA/CeO_2 Signal Tag. The preparation of the SiO_2@Au/dsDNA/CeO_2 signal tag is described in Scheme 1A. First of all, 0.5 mL of mixture solution containing 6 μM capture probe and 2 μM MPBA were dispersed into 1.5 mL of SiO_2@Au solution (details in the Supporting Information) for 12 h at room temperature. After that, the solution was treated with 5 μL of 2 mM HT for 1 h to remove the nonspecific binding and block the left active groups. Then, 10 μL of the 1 μM mixture of hairpin probe (DNA1 and DNA2) was incubated for 1 h to form DNA concatemer. Next, it was further incubated in 0.5 mL CeO_2 solution (details in the Supporting Information) containing EDC (50 mM) and NHS (50 mM) for another 2 h. After washing, the signal tag was ready for measurement.

2.3. Fabrication of the Boronate Affinity-Based MIPs Modified Electrodes. In order to improve the electron transport performance of the paper electrode, Au NRs was obtained by in-site growth on the surface of μPADs according to our previous works with slight modifications (details in the Supporting Information).[23] Next, ethanol–water solution (30:70, v/v) containing 200 μM MPBA was added in the modified electrode for 12 h at room temperature. Then, the residual reagent was removed by washing with ethanol and water and dried in air.

A thin template layer was carried out by introducing 10 mM of phosphate-buffered saline (PBS) buffer (pH 8.5) containing 0.5 mg·mL^{-1} of OVA into the boronic acid-functionalized electrodes at room temperature for 3 h. Then, a prepolymer mixture solution [regulate pH to ~9.3 with $NH_3 \cdot H_2O$ (28 wt %)] containing 0.5 mg·mL^{-1} of TMOS and 1.5 mg·mL^{-1} of PTEOS was injected into the template-anchored electrodes at room temperature for 12 h. Then, template molecules remain in the OVA imprinted Au–MPBA/MIPs surface could be removed by washing with HAc/NaAc solution (pH 4.0) several times. For comparison, preparation processes of nonimprinted polymers (NIPs) covered electrodes following the same method mentioned above but without the addition of OVA.

2.4. Electrochemical Detection Procedure of the Boronate Affinity Sandwich Assay. First, a 5 μL of OVA solutions of varying concentrations in 10 mM PBS (pH 8.5) was added into each MIP-modified paper sample zone of the μPADs, and each one was then incubated at room temperature for 30 min. Then, the electrode was incubated for 15 min with 5 μL of the SiO_2@Au/dsDNA/CeO_2 signal tag. The resulting electrodes were gently washed with deionized water for preventing the nonspecific binding and dried, and then DPV measurement was performed in 10 mM PBS (pH 7.4) from 0.0 to 0.6 V with a pulse amplitude of 50 mV, a pulse period of 0.2 s and a pulse width of 50 ms.

DOI: 10.1021/acsami.9b02005
ACS Appl. Mater. Interfaces XXXX, XXX, XXX–XXX

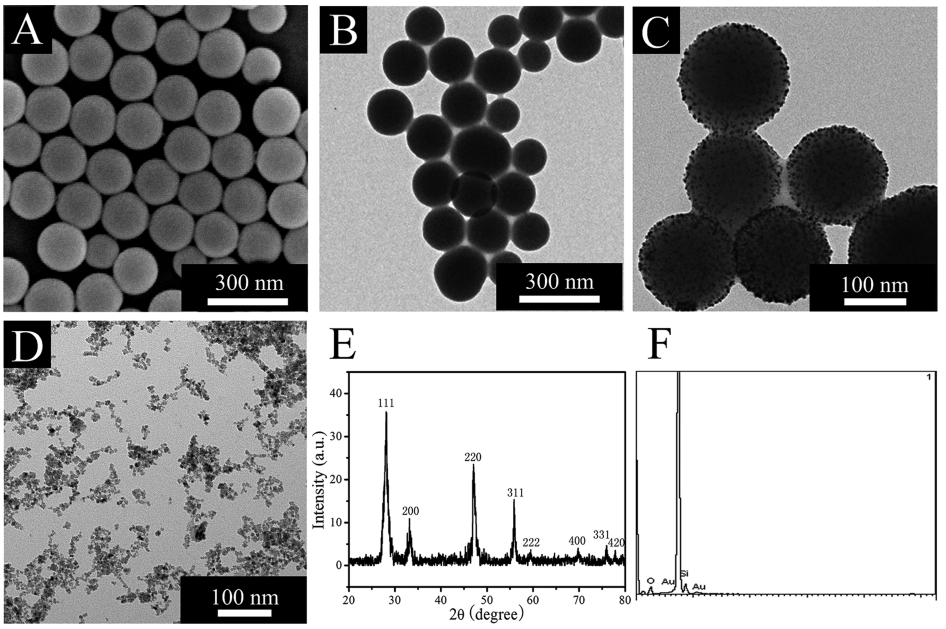

Figure 1. SEM (A) and TEM (B) images of SiO_2 NPs; TEM images (C) and EDS images (F) of SiO_2@Au; TEM images (D) and XRD pattern (E) of CeO_2.

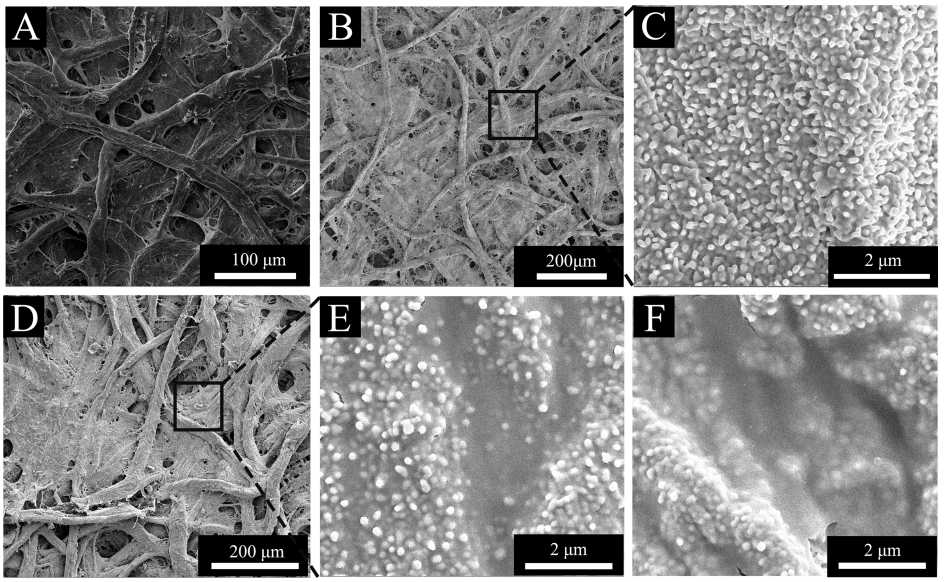

Figure 2. SEM images of (A) bare paper, (B) Au-μPADs, (C) further magnifications of (B), (D) MIPs modified Au-μPADs, (E) further magnifications of (D), and (F) NIPs modified Au-μPADs.

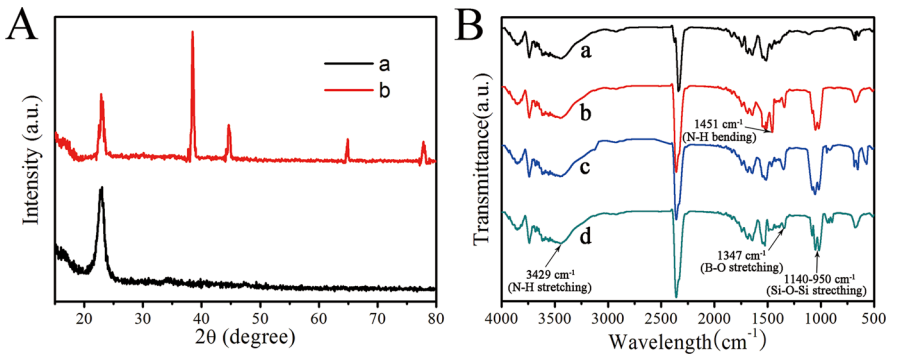

Figure 3. (A) XRD pattern of bare paper (a) and Au-μPADs (b); (B) FTIR spectra of Au-μPADs (a), Au-μPADs/MIPs (b), Au-μPADs/NIPs (c), and Au-μPADs/MIPs after removal of the template (d).

DOI: 10.1021/acsami.9b02005
ACS Appl. Mater. Interfaces XXXX, XXX, XXX−XXX

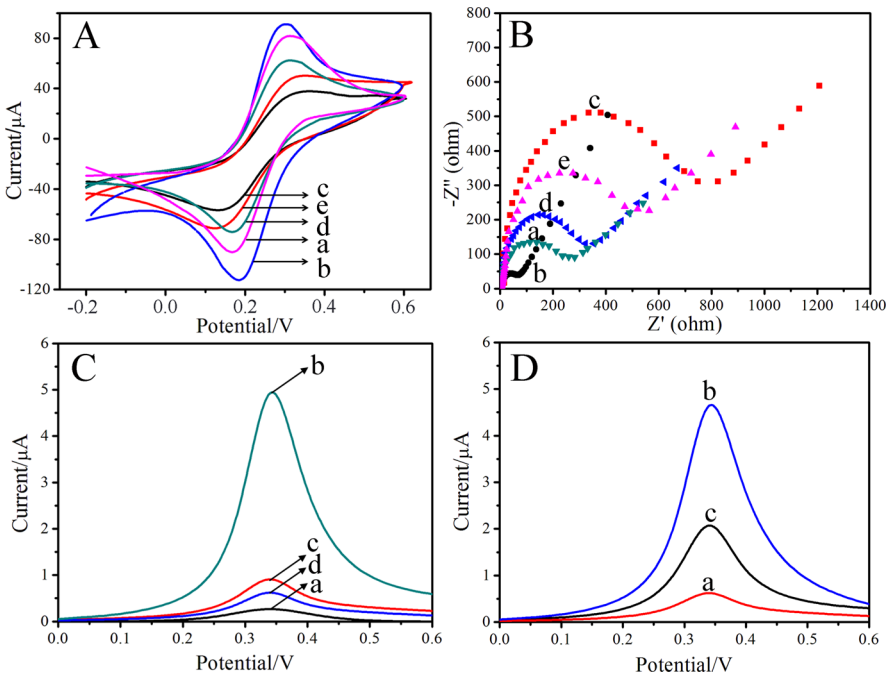

Figure 4. CV (A) and EIS (B) of μPADs (a), Au-μPADs (b), Au-μPADs/MIPs before (c) and after (d) template molecule extraction, and Au-μPADs/MIPs after rebinding of OVA (50 ng·mL^{-1}) (e), in 5 mM $K_3[Fe(CN)_6]/K_4[Fe(CN)_6]$ solution containing 0.1 M KCl. (C) DPV responses of Au-μPADs (a), Au-μPADs/MIPs (b), and Au-μPADs/NIPs (c) in 10 mM PBS (pH 7.4) with addition of 1000 ng/mL OVA and 0.5 mM 1-naphthol; Au-μPADs/MIPs (d) was processed in blank OVA in 10 mM PBS (pH 7.4). (D) DPV responses of MIPs-OVA-SiO_2@Au/dsDNA (a), MIPs-OVA-SiO_2@Au/dsDNA/CeO_2 (b), and MIPs-OVA-Au/dsDNA/CeO_2 (c) in 10 mM PBS (pH 7.4) in the presence of 1000 ng/mL OVA and 0.5 mM 1-naphthol.

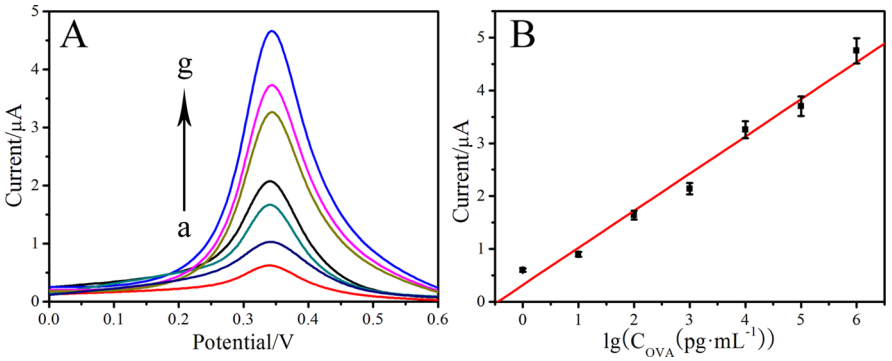

Figure 5. (A) DPVs of OVA detection with different concentrations in 10 mM PBS (pH 7.4) from 0.0 to 0.6 V with a pulse amplitude of 50 mV, a pulse period of 0.2 s, and a pulse width of 50 ms: 1 pg/mL, 10 pg/mL, 100 pg/mL, 1 ng/mL, 10 ng/mL, 100 ng/mL, 1000 ng/mL. (B) Corresponding calibration curve.

Table 1. Comparison of the Proposed Method with Other Approaches Published Earlier in Glycoprotein Detection

measurement method[a]	LOD	linear range	refs
SERS	10^{-6} μM	10^{-6} to 10^{-2} μM	41
FL	0.66 μM	1−10 μM	42
PEC	0.13 pg/mL	0.5 pg/mL to 10 μg/mL	43
ECL	3.3 pg/mL	0.01−10 ng/mL	44
electrochemistry	0.87 pg/mL	1 pg/mL to 1000 ng/mL	our work

[a]SERS, surface-enhanced Raman scattering; FL, fluorescence; PEC, photoelectrochemical; ECL, electrochemiluminescence.

3. RESULTS AND DISCUSSIONS

3.1. Characterization of the Synthesized Nanomaterials. Figure 1A,B shows the scanning electron microscopy (SEM) and transmission electron microscopy (TEM) images of the SiO_2 NPs, respectively. As we can see, a spherical structure of SiO_2 NPs with uniform size distribution and smooth surfaces was obtained from the SEM image. TEM presented morphology of SiO_2 NPs with an average diameter of about 140 nm (Figure S2A, details in the Supporting Information). As shown in Figure 1C, many small-sized Au NPs were visible as uniform and rough small black spots on the surface of SiO_2@Au in the presence of Na_3Cit. Furthermore, the energy-dispersive spectrometry (EDS) image is displayed in Figure 1F, providing evidence to illustrate the successful preparation of SiO_2@Au. Moreover, the morphologies of CeO_2 nanoparticles were characterized by TEM with a diameter

DOI: 10.1021/acsami.9b02005
ACS Appl. Mater. Interfaces XXXX, XXX, XXX−XXX

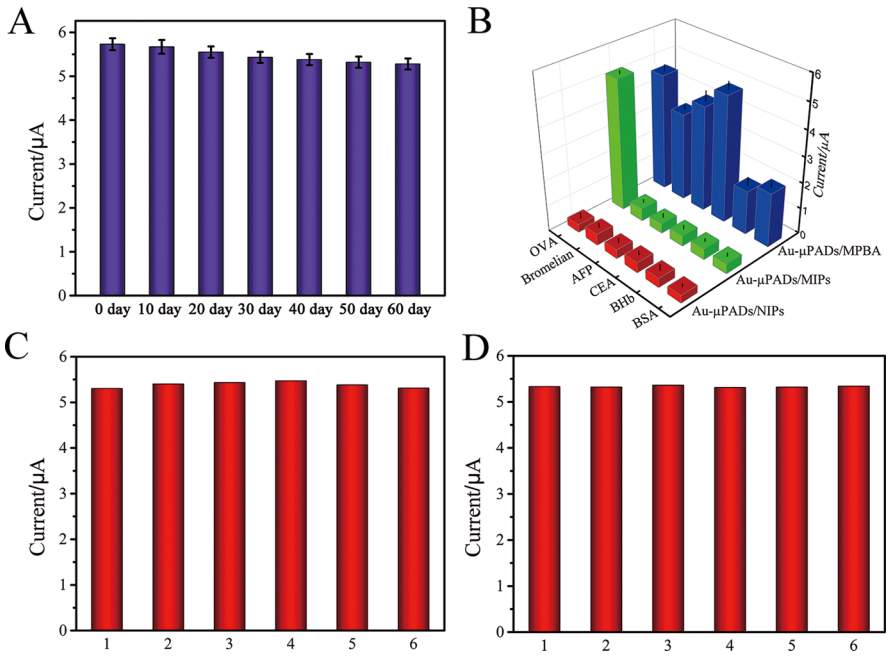

Figure 6. (A) Stability of the prepared biosensor at 4 °C. (B) Recognition ability of Au-μPADs/MPBA, Au-μPADs/MIPs, Au-μPADs/NIPs toward different proteins (OVA, bromelain, AFP, CEA, BHb, and BSA). (C) Reproducibility interassays of six biosensors prepared under the same conditions. (D) Reproducibility intraassays of one biosensor prepared in the same conditions.

Table 2. Determination of OVA in Chicken Egg White Samples Using the Proposed Sensing Platform

samples	added (ng/mL)	found (ng/mL)	RSD (%) (n = 3)	recovery (%)
1	0.5	0.52	2.5	102.0
2	1.0	1.03	2.7	103.0
3	1.5	1.45	2.8	96.6
4	2.0	2.02	2.6	101.0
5	2.5	2.38	2.5	95.2
6	3.0	2.95	2.3	98.3

about 10 nm (Figure S2B, details in the Supporting Information) as exhibited in Figure 1D. In addition, the X-ray diffraction (XRD) method was used to examine the phase and structure of synthesized CeO_2 nanoparticles in Figure 1E. The diffraction peaks around 28.5°, 33.0°, 47.4°, 56.3°, 59.3°, 69.8°, 75.9°, and 77.9° were observed, which corresponded to the (111), (200), (220), (311), (222), (400), (331), and (420) planes (JCPDS no. 34-0394) of fluorite-phase CeO_2.

3.2. Characterization of the Paper-Based Boronate-Affinity MIPs. As shown in Figure 2A, the chromatography paper was shown to have a framework of cellulosic fibers, which offered a biocompatible, incompact microenvironment for the immobilization of Au NRs. The two cellulose fibers were tightly connected at the points of contact, which might be attributed to hydrogen-bonding interactions of polysaccharides at the fiber. In order to improve the conductivity of the work electrode, a layer of Au NRs arrays were obtained on the paper work zone as depicted in Figure 2B. Based on the in situ growth mechanism, a close-knit and uniform growth of the Au NR conducting layer was observed after the Au seed successfully grows on the paper fiber.[40] The Au NR layer would enhance the area-to-volume ratio as well as increase the conductivity of the paper electrode to obtain a better electron transmission performance. A high-magnification SEM image is shown in Figure 2C, the prepared Au has a rod structure with a diameter of ∼20 nm, which was beneficial for enhancing the electron transfer rate. After the formation of MIPs on the surface of Au-μPADs, the SEM image of Au-μPADs/MIPs was obtained as shown in Figure 2D. Upon further magnification (Figure 2E), the Au-μPAD surface was wrapped with the intensive polymer layer, which demonstrates successful combination. The SEM image of Au-μPADs/NIPs was also obtained as depicted in Figure 2F.

In order to confirm the crystalline structure and phase purities of Au-μPADs and bare μPADs, the XRD analysis was performed as shown in Figure 3A. Compared with the XRD pattern of bare μPADs [curve (a)], Au-μPADs contained three characteristic diffraction peaks at about 38.4°, 44.4°, 64.8° [curve (b)], which correspond to the (111), (200), and (220) diffraction of cubic, respectively (JCPDS card no. 004-0784). Furthermore, Fourier transform infrared (FT-IR) which verifying the successful preparation of the boronate affinity molecularly imprinted film spectroscopy was obtained from KBr pressed pellets of the samples in Figure 3B. The FT-IR spectra of Au-μPADs, MIPs, NIPs, and MIPs after removal of the template were shown in curves (a–d), respectively. The spectra reveal a characteristic peak at approximately 3429 and 1451 cm^{-1} for the N–H bonding vibration of OVA. However, these bands were weaker in the spectra of NIPs and MIPs after removal of the template, indicating that glycoprotein successfully imprinted in the polymer film. In addition, the adsorption band of B–O stretching vibration appeared in 1347 cm^{-1}, providing the evidence that MPBA had been successfully modified onto Au-μPADs. Moreover, the bands between 1140 and 950 cm^{-1} can be attributed to Si–O–Si vibrations appeared in the spectrum of MIPs, NIPs, and MIPs after removal of the template. All these results confirmed that the MIPs were successfully prepared.

3.3. Electrochemical Characterization of the Proposed MIP Sensor. The surface properties of modified electrodes were characterized by CV and electrochemical

DOI: 10.1021/acsami.9b02005
ACS Appl. Mater. Interfaces XXXX, XXX, XXX–XXX

impedance spectroscopy (EIS) in Figure 4A,B. CV experiments were performed in 5.0 mM $K_3[Fe(CN)_6]/K_4[Fe(CN)_6]$ solution containing 0.1 M KCl with a scan rate of 50 mV/s as exhibited in Figure 4A. A pair of symmetric redox peaks of the biosensor appeared at the bare μPADs [curve (a)]. When Au NRs was introduced onto the μPADs surface, there was a remarkable increased redox peak current [curve (b)]. This might be attributed to the excellent electrical conductivity and electrocatalytic effect of the Au NRs, which serve as electroconductive material for improving the electron transfer rate of $[Fe(CN)_6]^{3-}$. The peak current of the electrode dramatically decreased from curve (b) to curve (c) after MIPs covered the surface of the electrode [curve (c)], which is possible to the electrostatic repulsion between the ferricyanide and MIPs toward the electrode surface. When the template molecules were removed from the MIPs [curve (d)], the current responses were enhanced as expected, accounting for the fact that the imprinting cavities could enhance the diffusion of $[Fe(CN)_6]^{3-}$. In comparison to curve (d), Au-μPADs/MIPs after rebinding of OVA exhibited lower peak current [curve (e)], which is likely a result of the combination of OVA and the MIP film. However, the peak current of curve (e) was still higher than that of curve (c), suggesting that OVA occupied a part of imprinting cavities. In addition, EIS has been reported to be a facile technique for characterizing the modified electrode surface during the sensor construction process. Each Nyquist diagram consisted of a semicircle at high frequency and a linear part at low frequency. The diameter of the semicircle was used to reflect the electron transfer resistance (R_{et}). Therefore, EIS was performed to investigate the electrochemical behaviors of the modified electrodes in 5.0 mM $[Fe(CN)_6]^{3-/4-}$ solution containing 0.1 M KCl as shown in Figure 4B. For bare μPADs, the impedance spectrum presented a relatively small semicircle [curve (a)] in a higher frequency range as a low R_{et}. After the modification of Au NRs, the Au-μPADs [curve (b)] exhibited a lower R_{et}, indicating that Au NRs have a stronger electronic transfer capability. However, with the boronate affinity-based oriented imprinting [curve (c)], the R_{et} was significantly increased. The results demonstrated that the MIPs film had low conductivities and great blocking effect, which produced a greater resistance to the electron transfer. Once the template was removed from the MIPs film [curve (d)], the R_{et} decreased obviously, indicating that the specific imprinted holes that appeared on the MIP film improved the electron transfer rate. While the MIP film was rebound with OVA [curve (e)], the R_{et} exhibited a significant increase, indicating that the OVA binding on the MIP film occupies site and hindering $[Fe(CN)_6]^{3-}$ redox probe from approaching the electrode surface.

To evaluate the performance of the proposed sensing platform, electrochemical detection toward OVA performed under the optimized experimental conditions (Figure S3, details in the Supporting Information). After preparing signal tag SiO_2@Au/dsDNA/CeO_2 to form the MIPs-OVA-tag sandwich assay in OVA solution (5 mL, 1000 ng/mL), the DPV intensity of Au-μPADs, Au-μPADs/MIPs, and Au-μPADs/NIPs were measured. In addition, in order to perform a controlled trial, the Au-μPADs/MIPs in the absence of OVA were electrochemically measured under the same condition. Figure 4C reveals the Au-μPADs [curve (a)] generating a negligible electrochemical signal after incubating in OVA. However, after modifying NIP [curve (c)], the current response was a little bit stronger than that of the Au-μPADs. This might be attributed to the fact that the polymer film-modified electrode surface adsorbed a few OVA. As revealed in curve (d), the DPV intensity of Au-μPADs/MIPs in blank OVA was also stronger compared to Au-μPADs. It might be because imprinting film pores adsorb a handful of electrochemical active substances. Afterward, expectedly, current intensity increased obviously when the signal tag was fixed on the electrode surface, indicating that the proposed sensing platform was successfully fabricated. Furthermore, in order to measure the performance of the prepared signal tag, the DPV peak currents of MIPs-OVA-SiO_2@Au/dsDNA, MIPs-OVA-SiO_2@Au/dsDNA/CeO_2, and MIPs-OVA-Au/dsDNA/CeO_2 were measured in 50 mg ng/mL OVA, 0.5 mM 1-naphthol, and 10 mM PBS (pH 7.4). As we can see in Figure 4D, the peak current was almost negligible when the electrode was incubated with SiO_2@Au/dsDNA [curve (a)] only because 1-naphthol cannot be oxidized in the absence of CeO_2. Thereafter, the peak current was enhanced significantly when the biosensor was incubated with SiO_2@Au/dsDNA/CeO_2 [curve (b)] owing to the excellent oxidation of CeO_2 toward 1-naphthol. More inspiringly, the current was significantly decreased when the sensing platform was incubated with Au/dsDNA/CeO_2 [curve (c)] instead of SiO_2@Au/dsDNA/CeO_2. The reason for this phenomenon was that the SiO_2 nanomaterial with a large surface area could carry large amounts of Au NPs, leading to signal amplification. The comparison results displayed that excellent signal tag (SiO_2@Au/dsDNA/CeO_2) was crucial to ultimately improve detection sensitivity.

3.4. Analytical Performance of the MIP Sensor. Under the optimal conditions (details in the Supporting Information), a series of different concentrations of OVA were measured to confirm the ability of the proposed sensor in 10 mM PBS (pH 7.4) from 0.0 to 0.6 V with a pulse amplitude of 50 mV, a pulse period of 0.2 s, and a pulse width of 50 ms. As depicted in Figure 5A, the DPV intensity gradually increased with the increase of target concentration because more signal tags were fixed on the electrode surface. A good linear relationship between DPV intensity and the logarithm of target OVA concentrations in the range of 1 pg/mL to 1000 ng/mL was displayed (Figure 5B). The regression equation was I (μA) = 2.555 lg C_{OVA} + 6.224 (R = 0.991) with a limit of detection (LOD) of 0.87 pg/mL (S/N = 3), where I and C represented the current intensity and OVA concentration, respectively. Additionally, Table 1 summarizes the performance of proposed work compared with that of some reported methods for glycoprotein detection. Our work represented an acceptable wider linear range and a lower detection limit, exhibiting its superior performance.

3.5. Stability, Reproducibility, and Selectivity of the Sensor. The long-time stability of this imprinted sensor was investigated by detection of the electrochemical signal change of the sensing electrode. Seven identical electrodes were constructed and then stored in 4 °C. It retained 92.1% of its original response value after a stored period of 60 days, indicating that the proposed sensor had good storage stability.

For the applications of imprinted materials, the recognition specificity was a key consideration factor for the designed biosensor. To examine selectivity of Au-μPADs/MIPs toward OVA, five kinds of proteins as interfering agents including bromelain, human α-fetoprotein (AFP), carcinoembryonic antigen (CEA), bovine hemoglobin (BHb), and bovine serum albumin (BSA) were chosen as the interferants. Figure

DOI: 10.1021/acsami.9b02005
ACS Appl. Mater. Interfaces XXXX, XXX, XXX−XXX

6B displays the electrode response of Au-μPADs/MIPs, Au-μPADs/NIPs, and Au-μPADs/MPBA toward these proteins under an equal concentration (1.0 ng/mL). Obviously, Au-μPADs/MIPs exhibited an evident increase response toward OVA than other proteins, indicating that a much higher binding capacity toward OVA was obtained. The current response of Au-μPADs/NIPs to OVA and other four proteins could be almost ignored compared with that of Au-μPADs/MIPs to OVA. Furthermore, in order to explore the influence of the boronate affinity interaction on the imprinting effect, the current intensity of Au-μPADs/MPBA was also measured in the presence of OVA. Au-μPADs/MPBA exhibited specific recognition toward all glycoproteins, illustrating that Au-μPADs/MPBA has no specific recognition function for protein. All these comparison results indicated that MIPs have excellent specific recognition property. Therefore, the excellent specific recognition of MIPs toward OVA was due to the combined action of boronate affinity of MPBA and the shape of the recognition sites in the imprinted matrix. These results suggested that the as-designed biosensor possessed a satisfied selectivity to OVA.

The reproducibility of the proposed sensor was investigated based on interassay precision and intraassay precision. The interassay precision was evaluated by measuring the 1.0 ng/mL of OVA on 6 different sensors independently. Meanwhile, 6-time parallel determination of 1.0 ng/mL of OVA from a single sensor was carried out to evaluate intraassay precision. A good reproducibility for preparing the sensors with the relative standard deviation (RSD) of interassay precision and intra-assay precision were 9.4 and 10.2%, respectively. Such reproducibility was highly acceptable for the as-designed sensing platform.

3.6. Application in the Real Chicken Egg White Sample. To evaluate the analytical reliability and the promising application potential of the constructed biosensor, a recovery experiment was performed by adding different concentrations of OVA (0.5, 1.0, 1.5, 2.0, 2.5, and 3.0 ng/mL) into 100-fold diluted egg white samples (Table 2). The obtained RSD was less than 2.8%, and the recoveries of OVA from egg white sample ranged from 95.2 to 103.0%, indicating that the proposed biosensor had an acceptable potential application for the detection of glycoproteins in real biological samples.

4. CONCLUSIONS

In summary, a paper-based biosensor successfully introduced boronate affinity sandwich assay for detecting OVA based on the SiO_2@Au/dsDNA/CeO_2 signal tag, which combined HCR and simultaneous achieving signal amplification. Furthermore, the introduction of boronate affinity MIPs effectively improved the selectivity of the proposed assay. In addition, the formation of hybridization chain and preparation of SiO_2@Au with a large surface area enhanced sensitivity of the sensing platform. Furthermore, nanoceria particles had an excellent catalytic property toward 1-naphthol, which could be oxidized into naphthoquinone. The proposed boronate affinity MIP sensor exhibited a wide linear range of 1 pg/mL to 1000 ng/mL, a low detection limit (0.87 pg/mL), and satisfying selectivity for OVA detection, which provide a promising platform for glycoprotein detection.

ASSOCIATED CONTENT

Supporting Information

The Supporting Information is available free of charge on the ACS Publications website at DOI: 10.1021/acsami.9b02005.

Materials and reagents; apparatus and measurements; all aptamer sequences used in the experiment; fabrication of the designed μPADs; preparation of SiO_2 NPs, SiO_2@Au, CeO_2 nanoparticles, and Au-μPADs; optimized of detection conditions (PDF)

AUTHOR INFORMATION

Corresponding Authors

*E-mail: chm_gesg@163.com. Phone: +86-531-82767161. Fax: +86-531-82765956 (S.G.).
*E-mail: chm_yanm@ujn.edu.cn (M.Y.).

ORCID

Shenguang Ge: 0000-0002-0537-6491
Jinghua Yu: 0000-0001-5043-0322

Notes

The authors declare no competing financial interest.

ACKNOWLEDGMENTS

This work was financially supported by the National Natural Science Foundation of China (21575051, 21775055, 21874055); the Key Research and Development Program of Shandong Province, China (2018GGX103037); and the Taishan Scholars Program (ts201712048).

REFERENCES

(1) Mochizuki, K.; Molinero, V. Antifreeze Glycoproteins Bind Reversibly to Ice via Hydrophobic Groups. *J. Am. Chem. Soc.* **2018**, *140*, 4803−4811.

(2) Qu, X.; Wang, F.; Sun, Y.; Tian, Y.; Chen, R.; Ma, X.; Liu, C. Selective Extraction of Bioactive Glycoprotein in Neutral Environment through Concanavalin a Mediated Template Immobilization and Dopamine Surface Imprinting. *RSC Adv.* **2016**, *6*, 86455−86463.

(3) Cao, X.; Kang, S.; Yang, M.; Li, W.; Wu, S.; Han, H.; Meng, L.; Wu, R.; Yue, X. Quantitative N-glycoproteomics of Milk Fat Globule Membrane in Human Colostrum and Mature Milk Reveals Changes in Protein Glycosylation during Lactation. *Food Funct.* **2018**, *9*, 1163−1172.

(4) Stephenson-Brown, A.; Acton, A. L.; Preece, J. A.; Fossey, J. S.; Mendes, P. M. Selective Glycoprotein Detection Through Covalent Templating and Allosteric Click-imprinting. *Chem. Sci.* **2015**, *6*, 5114−5119.

(5) Dube, D. H.; Champasa, K.; Wang, B. Chemical Tools to Discover and Target Bacterial Glycoproteins. *Chem. Commun.* **2011**, *47*, 87−101.

(6) Zhu, Z.; Zhou, X.; Wang, Y.; Chi, L.; Ruan, D.; Xuan, Y.; Cong, W.; Jin, L. Fluorescent Staining of Glycoproteins in Sodium Dodecyl Sulfate Polyacrylamide gels by 4H-[1]-benzopyrano[4,3-b]thiophene-2-carboxylic acid hydrazide. *Analyst* **2014**, *139*, 2764−2773.

(7) Chaffey, P. K.; Guan, X.; Li, Y.; Tan, Z. Using Chemical Synthesis To Study and Apply Protein Glycosylation. *Biochemistry* **2018**, *57*, 413−428.

(8) Reatini, B. S.; Ensink, E.; Liau, B.; Sinha, J. Y.; Powers, T. W.; Partyka, K.; Bern, M.; Brand, R. E.; Rudd, P. M.; Kletter, D.; Drake, R.; Haab, B. B. Characterizing Protein Glycosylation through On-Chip Glycan Modification and Probing. *Anal. Chem.* **2016**, *88*, 11584−11592.

(9) Wang, Y.; Hai, X.; E, S.; Chen, M.; Yang, T.; Wang, J. Boronic Acid Functionalized g-C_3N_4 Nanosheets for Ultrasensitive and Selective Sensing of Glycoprotein in the Physiological Environment. *Nanoscale* **2018**, *10*, 4913−4920.

DOI: 10.1021/acsami.9b02005
ACS Appl. Mater. Interfaces XXXX, XXX, XXX−XXX

(10) Wu, J.; Xie, X.; Liu, Y.; He, J.; Benitez, R.; Buckanovich, R. J.; Lubman, D. M. Identification and Confirmation of Differentially Expressed Fucosylated Glycoproteins in the Serum of Ovarian Cancer Patients Using a Lectin Array and LC-MS/MS. *J. Proteome Res.* **2012**, *11*, 4541−4552.
(11) Capoferri, D.; Ávarez-Didukr, R.; Del Carlo, M.; Compagnone, D.; Merkoçi, A. Electrochromic Molecular Imprinting Sensor for Visual and Smartphone-Based Detections. *Anal. Chem.* **2018**, *90*, 5850−5856.
(12) Pei, D.-N.; Zhang, A.-Y.; Pan, X.-Q.; Si, Y.; Yu, H.-Q. Electrochemical Sensing of Bisphenol A on Facet-Tailored TiO_2 Single Crystals Engineered by Inorganic-Framework Molecular Imprinting Sites. *Anal. Chem.* **2018**, *90*, 3165−3173.
(13) Ben-Amram, Y.; Riskin, M.; Willner, I. Selective and Enantioselective Analysis of Mono- and Disaccharides using Surface Plasmon Resonance Spectroscopy and Imprinted Boronic Acid-functionalized Au Nanoparticle Composites. *Analyst* **2010**, *135*, 2952−2959.
(14) Xu, S.; Lu, H. Ratiometric Fluorescence and Mesoporous Structure Dual Signal Amplification for Sensitive and Selective Detection of TNT Based on MIP@QD Fluorescence Sensors. *Chem. Commun.* **2015**, *51*, 3200−3203.
(15) Lim, G. W.; Lim, J. K.; Ahmad, A. L.; Chan, D. J. C. Fluorescent Molecularly Imprinted Polymer Based on Navicula sp. Frustules for Optical Detection of Lysozyme. *Anal. Bioanal. Chem.* **2016**, *408*, 2083−2093.
(16) Beluomini, M. A.; da Silva, J. L.; Stradiotto, N. R. Amperometric Determination of Myo-inositol by using a Glassy Carbon Electrode Modified with Molecularly Imprinted Polypyrrole, Reduced Graphene Oxide and Nickel Nanoparticles. *Microchim. Acta* **2018**, *185*, 170.
(17) Çrmanv, M. E.; Armutcu, C.; Uzun, L.; Say, R.; Denizli, A. Self-oriented Nanoparticles for Site-selective Immunoglobulin G Recognition via Epitope Imprinting Approach. *Colloids Surf., B* **2014**, *123*, 831−837.
(18) Yang, X.; Dong, X.; Zhang, K.; Yang, F.; Guo, Z. A Molecularly Imprinted Polymer as an Antibody Mimic with Affinity for Lysine Acetylated Peptides. *J. Mater. Chem. B* **2016**, *4*, 920−928.
(19) Chen, H.; Kong, J.; Yuan, D.; Fu, G. Synthesis of Surface Molecularly Imprinted Nanoparticles for Recognition of Lysozyme using a Metal Coordination Monomer. *Biosens. Bioelectron.* **2014**, *53*, 5−11.
(20) Wang, S.; Ye, J.; Bie, Z.; Liu, Z. Affinity-tunable Specific Recognition of Glycoproteins via Boronate Affinity-based Controllable Oriented Surface Imprinting. *Chem. Sci.* **2014**, *5*, 1135.
(21) Bi, X.; Liu, Z. Facile Preparation of Glycoprotein-Imprinted 96-Well Microplates for Enzyme-Linked Immunosorbent Assay by Boronate Affinity-Based Oriented Surface Imprinting. *Anal. Chem.* **2014**, *86*, 959−966.
(22) Bi, X.; Liu, Z. Enzyme Activity Assay of Glycoprotein Enzymes Based on a Boronate Affinity Molecularly Imprinted 96-Well Microplate. *Anal. Chem.* **2014**, *86*, 12382−12389.
(23) Sun, X.; Wang, H.; Jian, Y.; Lan, F.; Zhang, L.; Liu, H.; Ge, S.; Yu, J. Ultrasensitive Microfluidic Paper-based Electrochemical/Visual Biosensor based on Spherical-like Cerium Dioxide Catalyst for MiR-21 Detection. *Biosens. Bioelectron.* **2018**, *105*, 218−225.
(24) Cunningham, J. C.; Brenes, N. J.; Crooks, R. M. Paper Electrochemical Device for Detection of DNA and Thrombin by Target-induced Conformational Switching. *Anal. Chem.* **2014**, *86*, 6166−6170.
(25) Scida, K.; Li, B.; Ellington, A. D.; Crooks, R. M. DNA Detection using Origami Paper Analytical Devices. *Anal. Chem.* **2013**, *85*, 9713−9720.
(26) Martinez, A. W.; Phillips, S. T.; Butte, M. J.; Whitesides, G. M. Patterned Paper as a Platform for Inexpensive, Low-Volume, Portable Bioassays. *Angew. Chem., Int. Ed.* **2007**, *46*, 1318−1320.
(27) Martinez, A. W.; Phillips, S. T.; Whitesides, G. M. Three-dimensional Microfluidic Devices Fabricated in Layered Paper and Tape. *Proc. Natl. Acad. Sci. U.S.A.* **2008**, *105*, 19606−19611.
(28) Wang, H.; Jian, Y.; Kong, Q.; Liu, H.; Lan, F.; Liang, L.; Ge, S.; Yu, J. Ultrasensitive Electrochemical Paper-based Biosensor for MicroRNA via Strand Displacement Reaction and Metal-organic Frameworks. *Sens. Actuators, B* **2018**, *257*, 561−569.
(29) Xu, Q.; Zhu, G.; Zhang, C.-y. Homogeneous Bioluminescence Detection of Biomolecules Using Target-Triggered Hybridization Chain Reaction-Mediated Ligation without Luciferase Label. *Anal. Chem.* **2013**, *85*, 6915−6921.
(30) Chang, Y.; Zhuo, Y.; Chai, Y.; Yuan, R. Host−Guest Recognition-Assisted Electrochemical Release: Its Reusable Sensing Application Based on DNA Cross Configuration-Fueled Target Cycling and Strand Displacement Reaction Amplification. *Anal. Chem.* **2017**, *89*, 8266.
(31) Wang, Y.; Bai, J.; Huo, B.; Yuan, S.; Zhang, M.; Sun, X.; Peng, Y.; Li, S.; Wang, J.; Ning, B.; Gao, Z. Upconversion Fluorescent Aptasensor for Polychlorinated Biphenyls Detection Based on Nicking Endonuclease and Hybridization Chain Reaction Dual-Amplification Strategy. *Anal. Chem.* **2018**, *90*, 9936−9942.
(32) Voiry, D.; Yamaguchi, H.; Li, J.; Silva, R.; Alves, D. C. B.; Fujita, T.; Chen, M.; Asefa, T.; Shenoy, V. B.; Eda, G.; Chhowalla, M. Enhanced catalytic activity in strained chemically exfoliated WS_2 nanosheets for hydrogen evolution. *Nat. Mater.* **2013**, *12*, 850.
(33) Wei, H.; Wang, E. Nanomaterials with Enzyme-like Characteristics (nanozymes): Next-generation Artificial Enzymes. *Chem. Soc. Rev.* **2013**, *42*, 6060−6093.
(34) Varga, E.; Pusztai, P.; Óiszt, L.; Oszkó, A.; Erdőhelyi, A.; Papp, C.; Steinrück, H.-P.; Kónya, Z.; Kiss, J. Probing the Interaction of Rh, Co and Bimetallic Rh−Co Nanoparticles with the CeO_2 Support: Catalytic Materials for Alternative Energy Generation. *Phys. Chem. Chem. Phys.* **2015**, *17*, 27154−27166.
(35) Yao, T.; Tian, Z.; Zhang, Y.; Qu, Y. Phosphatase-like Activity of Porous Nanorods of CeO_2 for the Highly Stabilized Dephosphorylation under Interferences. *ACS Appl. Mater. Interfaces* **2019**, *11*, 195−201.
(36) Sun, C.; Li, H.; Chen, L. Nanostructured Ceria-based Materials: Synthesis, Properties, and Applications. *Energy Environ. Sci.* **2012**, *5*, 8475.
(37) Hayat, A.; Andreescu, S. Nanoceria Particles as Catalytic Amplifiers for Alkaline Phosphatase Assays. *Anal. Chem.* **2013**, *85*, 10028−10032.
(38) Djuričić, B.; Pickering, S. Nanostructured Cerium Oxide: Preparation and Properties of Weakly-agglomerated Powders. *J. Eur. Ceram. Soc.* **1999**, *19*, 1925−1934.
(39) Wang, H.; Zhou, C.; Sun, X.; Jian, Y.; Kong, Q.; Cui, K.; Ge, S.; Yu, J. Polyhedral-AuPd Nanoparticles-based Dual-mode Cytosensor with Turn on Enable Signal for Highly Sensitive Cell Evalution on Lab-on-paper Device. *Biosens. Bioelectron.* **2018**, *117*, 651−658.
(40) Yang, H.; Zhang, Y.; Li, L.; Sun, G.; Zhang, L.; Ge, S.; Yu, J. Real-time and in Situ Enzyme Inhibition Assay for the Flux of Hydrogen Sulfide Based on 3D Interwoven AuPd-reduced Graphene Oxide Network. *Biosens. Bioelectron.* **2017**, *87*, 53−58.
(41) Xie, D.; Zhu, W. F.; Cheng, H.; Yao, Z. Y.; Li, M.; Zhao, Y. L. An Antibody-free Assay for Simultaneous Capture and Detection of Glycoproteins by Surface Enhanced Raman Spectroscopy. *Phys. Chem. Chem. Phys.* **2018**, *20*, 8881−8886.
(42) Guo, T.; Deng, Q.; Fang, G.; Yun, Y.; Hu, Y.; Wang, S. A Double Responsive Smart Upconversion Fluorescence Sensing Material for Glycoprotein. *Biosens. Bioelectron.* **2016**, *85*, 596−602.
(43) Li, Y.-J.; Ma, M.-J.; Zhu, J.-J. Dual-Signal Amplification Strategy for Ultrasensitive Photoelectrochemical Immunosensing of α-Fetoprotein. *Anal. Chem.* **2012**, *84*, 10492−10499.
(44) Cao, Y.; Yuan, R.; Chai, Y.; Mao, L.; Yang, X.; Yuan, S.; Yuan, Y.; Liao, Y. A Solid-State Electrochemiluminescence Immunosensor Based on MWCNTs-Nafion and $Ru(bpy)_3^{2+}$/Nano-Pt Nanocomposites for Detection of α-Fetoprotein. *Electroanalysis* **2011**, *23*, 1418−1426.

DOI: 10.1021/acsami.9b02005
ACS Appl. Mater. Interfaces XXXX, XXX, XXX−XXX